Journal of Cluster Science (2020) 31:1041–1050
https://doi.org/10.1007/s10876-019-01709-2

ORIGINAL PAPER

Photobiosynthesis of Silver Nanoparticle Using Extract of *Aspergillus flavus* CR500: Its Characterization, Antifungal Activity and Mechanism Against *Sclerotium rolfsii* and *Rhizoctonia solani*

Deepa Kanaujiya[1] · Vinay Kumar[1] · S. K. Dwivedi[1] · Ganesh Prasad[1]

Received: 14 September 2019 / Published online: 5 November 2019

Abstract
Newly biosynthesized metallic nanoparticle with antimicrobial characteristic attracted its demand in the field of disease management. The present study deals with the synthesis of silver nanoparticle using the extract *Aspergillus flavus* CR500 under the presence of sunlight. The characterization via scanning and transmission electron microscope revealed their size distribution ranges from 60 to 130 nm with a high content of Ag, confirmed by energy dispersive X-ray spectroscopic analysis. X-ray diffraction and Fourier transform infrared analysis exposed the crystalline nature and active functional group availability on silver nanoparticle (AgNPs). Photobiosynthesized AgNPs have high antimicrobial property and completely inhibited the growth of plant pathogenic fungi *Rhizoctonia solani* GPB and *Sclerotium rolfsii* at the concentration of 150 and 300 µg/L respectively. AgNPs exposure increases the lipid peroxidation (via reactive oxygen species production) in *R. solani* and *S. rolfsii*, might be a primary cause of AgNPs toxicity to fungal cell. However, fungal cell responded to oxidative stress caused by AgNPs by increasing the catalase and peroxidase activity. In order to assess the AgNPs applicability in seed protection and its impact on germination, growth and development of the crop, *Cicer arietinum* and *Vigna radiata* seeds were used for growth and germination assay under AgNPs exposure.

Keywords Nanoparticle · Shape and size of AgNPs, Antifungal mechanism · Oxidative stress · Antioxidants

Introduction

In recent year, the demand of newly synthesized silver nanoparticles (AgNPs) has been significantly increased for the application in the agricultural and industrial sectors. The antimicrobial (antibacterial, antifungal and antiviral activity) property of AgNPs is major cause of considerable attraction for its potential use in controlling the bacterial, fungal and viral pathogen in medical, industrial and agriculture field [1–4]. These days agriculture being challenged due to insect and pathogen (fungi and bacteria) attack [5] and the ability to adopt the stress conditions, the pathogens adopted resistance against traditional pesticides resulting spectacular crop loss [6, 7]. Chemical pesticide is also eco-destructive, persistent in nature, affect to soil micro-biota and causes number of human health issues. In this regards, there is need of novel strategies to control the pathogen and improve agriculture productivity. The implementation of nanoparticle in the agriculture sector is believed as navel strategies to deal with plant pathogen that will transform agricultural performance and help to improve crop productivity [5].

The chemical based synthesis of metallic nanoparticle is associated with number of disadvantages at all the stages due to applying toxic chemically originated organic solvents, reducing agents, and stabilizers, consequently are not environmental friendly [3, 8]. However, the green synthesis of nanoparticle can remove the disadvantages. The biologically originated bioactive materials from various sources such as microbes (bacteria and fungi) and plant (plant extract) are being utilized for synthesis of AgNPs, having potential antimicrobial activity [4, 9–12]. Fungal mediated synthesis of metallic nanoparticle is described to be more compensation than using bacteria in the processes

Deepa Kanaujiya and Vinay Kumar contributed for first author.

✉ S. K. Dwivedi
skdwivedibbau@gmail.com

[1] Department of Environmental Science, Babasaheb Bhimrao Ambedkar University, Lucknow 226025, India

[13]. Fungal species such as *Fusarium chlamydosporum*, *Penicillium chrysogenum* [14], *Macrophomina phaseolina* [5], *Aspergillus flavus* [15] have been reported for their ability to synthesize AgNPs. Fungi produce reductive agents such as enzymes and proteins that could operate reduction of Ag+ and synthesizes nanoparticles [5, 13, 16, 17].

Interestingly, the nanoparticle is an emerging field in the application as antimicrobial agents, but the antimicrobial mechanism is still unknown. However, some researchers have suggested that oxidative stress (reactive oxygen species production) generated by AgNPs inside the cell of the microorganism is the primary cause of its toxicity and antimicrobial activity [18, 19]. Spagnoletti et al. [5] reported that AgNPs exposure causes oxidative stress by generating reactive oxygen species (ROS) in *E. coli* resulting in cell death. Similar result was reported in *Phanerochaete chrysosporium* and at the lower concentration of AgNPs resultant oxidative stress evoked by antioxidants response (catalase; CAT, peroxidase; POD, superoxide dismutase; SOD and glutathione; GSH) while higher concentration of AgNPs causes cell death [12]. Lipid peroxidation via ROS has also been reported in algae, higher plant, Zebrafish and rat [20–23].

The present study deals with photobiosynthesis of AgNPs using the extract of *Aspergillus flavus* CR500, its characterization (via SEM–EDS; scanning electron microscope-energy dispersive X-ray spectroscope, TEM; transmission electron microscope, FTIR; Fourier transform infrared spectroscopy and XRD; X-ray diffraction), and antifungal activity. To get insights the antifungal mechanism, AgNPs exposed mycelia of selected plant pathogenic fungi subjected to oxidative stress and antioxidants response analysis showed considerable changes. To assess the applicability of AgNPs for seed protection via coating and also get to know the negative impact of AgNPs on crop development, its effect on seed germination rate, growth and biochemical response of the plant was analyzed using *Vigna radiata* and *Cicer arietinum* seeds.

Materials and Method

Photobiosynthesis of AgNPs from Extract of *Aspergillus flavus* CR500

The fungus *Aspergillus flavus* CR500 used for the synthesis of AgNPs, was previously isolated by Kumar and Dwivedi [24]. The isolate was periodically sub-cultured on potato dextrose agar (PDA) (HiMedia, Mumbai, India) plate and stored at room temperature.

Two hundred mL Potato Dextrose Broth (PDB) (HiMedia, Mumbai, India) was taken in 500 mL Erlenmeyer flask. The flask was inoculated with 3×10^7 spore suspension of *Aspergillus flavus* CR500 and incubated at 28 ± 1 °C in an incubator shaker at 80 rpm. After seventh day of incubation, the obtained culture was centrifuged at 3000 rpm for 10 min at 4 °C and the supernatant was employed as extract. The obtained extract (20 mL) was mixed with an equal amount (20 mL) of 50 mM $AgNO_3$ (Molychem, Mumbai, India) solution prepared in distilled water and equally divided in two vial tubes. One tube was incubated in dark condition at room temperature and another vial tube was incubated under sunlight for 2 h where the temperature was 32 °C and sunlight 800 Wm^{-2} which was measured using digital solar power meter, Kusam-meco (model; KM-SPM-530). After incubating the mixture under the sunlight, the colour of the mixture was converted into reddish brown within 10 min and completely changed in dark reddish black in 2 h of the reaction time, while no change in colour was observed in mixture incubated in dark condition up to 2 h of reaction period. To confirm the AgNPs synthesis, the absorbance of mixture was scanned using UV–visible spectrophotometer (Varian: Cary 100 Bio). The obtained mixture (incubated under sunlight) was centrifuged at 12,000 rpm for 10 min at 4 °C. The supernatant was discarded and AgNPs was dried at 40 °C for 10 h and stored at room temperature in a tightly closed vial tube and to avoid moisture.

Characterization of Synthesized AgNPs

Electron Microscopy Analysis

Electron microscope analysis was carried out using SEM (JEOL, Japan; model JSM-6490LV) coupled with Energy dispersive X-ray spectrophotometer (EDS). The oven dried (40 °C for 10 h) AgNPs was mounted on aluminium studs using carbon tape and coated with platinum and analyzed for shape determination. For the TEM analysis, sample was directly mounted on the Copper grid and the size dimension of the AgNPs was analysed using transmission electron microscope (JEOL).

XRD Analysis

To determine the crystalline structure in synthesized AgNPs, the X-ray diffraction analysis of oven dried AgNPs (40 °C for 10 h) was performed using Rigaku, X-ray diffractometer (Model: Mini flex 600).

FTIR Spectroscopy

IR spectrum of the synthesized silver nanoparticles was analyzed using Fourier transform infrared spectroscopy (Thermo Scientific Nicole 6700, USA). For the FTIR

characterization, the sample was mixed with solid KBr (potassium bromide) uniformly and properly which was compressed with hydraulic press to form thin transparent pellets and was used for FTIR analysis. The IR absorbance of the sample was recorded in the wavelength ranges from 4000 to 400 cm^{-1} [25].

Antifungal Activity Against Plant Pathogenic Fungi

Plant Pathogenic Fungi

The plant pathogenic fungus *Sclerotium rolfsii* was isolated by Prasad and Dwivedi [26] and periodically sub-cultured on PDA plate and stored at room temperature. Before use, the isolate was revived on PDA at least three times.

For the isolation of the fungus *Rhizoctonia solani* GPB, the rhizospheric soil of infected maize plant was collected from Bijanaur, Near BBAU Campus, Lucknow, India (26°44′05″ N and 80°54′23″ E). The serial dilution was made up to 10^{-3} and 0.1 mL of aliquot of each dilution was spread on PDA plate separately. To avoid the bacterial contamination, the plates were amended with 0.1% of streptomycin and incubated at 28 ± 1 °C in an incubator for 6 days. The grown fungal colonies were morphologically analyzed using the microscopic technique with the help of available literature. For the molecular identification, the genomic DNA was isolated using standard phenol/chloroform extraction method [27] followed by PCR amplification using universal primers ITS1 [5′-TCCGTAGGTGAACCTGCGG-3′] and ITS4 [5′-TCCTCCGCTTATTGATATGC-3′] [28]. The purified PCR product was directly sequenced on an ABI® 3730XL automated DNA Sequencer (Applied Biosystems, Inc., Foster City, CA) as per manufacturer's instructions. For identification, the sequenced data were analyzed and assembled using BLAST (Basic Local Alignment Search Tool; https://blast.ncbi.nlm.nih.gov/Blast.cgi) NCBI (National Center for Biotechnology Information) [29]. To assess the confidence limits of the branching, bootstrap analysis was performed. The ITS region sequence was deposited to NCBI database under accession number MK621284. The neighbour-joining tree was reconstructed using a standard parameter of CLUSTAL W (on MEGA X software) alignment with a gap opening penalty 15 and gap extension penalty of 6.66 for both pair wise alignment and multiple alignments [30].

Antifungal Assay

The Antifungal activity was assayed using the plate dilution method. AgNPs (30, 150, 300, 500 µg/L) amended PDA medium was poured into 90 mm diameter of Petri plates separately. AgNPs amended plates were inoculated with 0.5 cm diameter of seventh-day old culture of *Sclerotium rolfsii* and *Rhizoctonia solani* GPB separately and the plates were incubated for 6 days at 28 ± 1 °C. The growth of the colony diameter was measured regularly at second, fourth and sixth day. The inhibition percentage was calculated using the following equation.

$$Ip = \frac{R - r}{R} \times 100 \quad (1)$$

where Ip: inhibition percentage, R: radial growth of fungal on without AgNPs amended PDA plate, r: radial growth of fungal colony on AgNPs amended PDA plate.

Lipid Peroxidation and Antioxidant Response Analysis in Fungi Grown Under AgNPs Exposure

For the lipid peroxidation, 6 days grown mycelial biomass was harvested from different concentration of AgNPs (0, 20 and 50 µg/L) amended PDB medium. Melondialdehyde (MDA), the marker of lipid peroxidation was determined by following the method explained by Zhang et al. [31]. For the antioxidants response analysis, the activity of catalase (CAT) [32] and peroxidase (POD) [33] was analyzed in pathogenic fungi grown in presence of different concentration of AgNPs.

Effect of AgNPs on *V. radiata* and *C. arietinum*

Germination Rate and Growth Test

Vigna radiata and *Cicer arietinum* seeds were surface sterilized using 1% sodium hypochloride for 2 min [34]. For germination test, 5 seeds of *V. radiata* and *C. arietinum* were placed at equidistance in Petri plate containing sterilized doubled layered Whatman No. 1 filter paper separately. The plates were watered at alternate day with 10 mL of 500 and 1000 µg/L of AgNPs separately. Control set was also prepared and watered with sterilized distilled water. All the treatments were made in triplicates and incubated for 7 days at room temperature. The length of shoot and root was measured and the germination rate was calculated using the following formula [35]:

$$Germination\ Rate = \frac{Number\ of seeds\ germinated}{Total\ number\ of\ seeds} \times 100$$

Estimation of Lipid Peroxidation and Proline Content

The shoot of *Vigna radiata* and *Cicer arietinum* was harvested from the growth and germination test experiment at different concentration of AgNPs at seventh day after

incubation and the lipid peroxidation [36] and proline content [37] were estimated.

Data Analysis

Evolutionary analysis of isolate GPB was conducted on MEGA X [30]. Data were analyzed by analysis of variance (ANOVA) using SPSS software version 20.0 the means of the data were compared using post hoc test (Duncan Multiple Range Test; $DMRT_{(P \leq 0.05)}$).

Results and Discussion

Characterization of Photobiosynthesized AgNPs

UV–Visible Spectroscopic Analysis

During the initial experiment of the synthesis of AgNPs, no change in the colour observed in the mixture incubated in dark condition even after 2 h of incubation period, while the mixture incubated under sunlight was changed in reddish black, the sign of silver nanoparticle synthesis. For the confirmation of synthesis of AgNPs, the change in the colour of the sample (incubated under sunlight) from transparent to dark reddish black colour was scanned in the spectral band ranged from 350 to 700 nm using UV–visible spectrophotometer. The appearance of the sharp peak at 405 nm is the indication of AgNPs synthesis (Fig. 2a), which is due to Surface Plasmon Resonance (SPR) in synthesized nanoparticles [38, 39]. However, the colour change due to SPR phenomenon depends on nanoparticle size, its concentration and reducing material [39, 40].

SEM/EDX Analysis of Silver Nanoparticles

The determination of size and shape of AgNPs were analyzed by SEM analysis. SEM images showed individual AgNPs as well as a number of aggregates. The particle size of the synthesized nanoparticles was about 67–120 nm. 120 nm is dominated above individual cubical particles (Fig. 1a, b). The shape of the biosynthesized AgNPs was cubical and spherical with irregular surface. SEM images showed that the AgNPs are stable and in direct contact. Aggregated nanoparticles with larger irregular structure and no well-defined morphology were also found. The AgNPs synthesis with size ranges from 10 to 40 nm was reported in *Pleurotus ostreatus* [41]. Guilger et al. [34] reported the AgNPs production by *Trichoderma harzianum* and determined the average size from 20 to 30 nm with spherical shape using SEM analysis. In the present study, the EDX analysis showed a strong peak around 3.0 keV corresponds to the binding energies of Ag (Fig. 1c) which indicated that the synthesized nanoparticles were composed of high purity of Ag nanoparticles. The EDX result also shows the presence of Carbon, Oxygen, Sodium, Aluminium and Magnesium. Moreover, the weight % of Ag was recognized 9.80 on EDX analysis that confirmed the presence of AgNPs in the synthesized nanoparticle. The presence of Ag in nanoparticles was also reported in synthesized silver nanaoparticles from different sources to confirm the presence of Ag [34, 42–44].

FTIR Analysis

For the assessment of the possible functional groups present on the synthesized silver nanoparticles, the FTIR analysis was performed. The observed peaks are shown in Fig. 2b and their assigned functional groups are listed in Table 1. The peak observed at 3444.7 cm^{-1} denotes the O–H and N–H stretching. The strong peak recorded at 1636.2 cm^{-1} denotes the presence of C=O stretching [45, 46]. The band at 1382.6 cm^{-1} denotes the –COOH stretching. The absorption band at 1092.5 cm^{-1} represents to the phosphate group stretching and the band at 609.2 cm^{-1} assigned to the bending SO_2 stretching. The functional groups such as COOH, C=O, N–H groups present in the sample might be responsible for the bioreduction of Ag^+ to AgNPs [46, 47]. According to Basavaraja [48], amino acids and carbonyl group in peptide bond of protein strongly bind the metal and probably form a coating on the metal synthesized nanoparticles.

XRD Analysis

The XRD analysis determined the presence of the crystalline structure in the synthesized AgNPs. Figure 1d shows the XRD pattern of prepared AgNPs by the extract of *A. flavus* CR500, which shows major peaks at 2θ positions of 24.4°, 37.31° and 64.3° representing the diffraction plane (222), (111) and (220) respectively [49–51]. These results revealed the crystalline nature of AgNPs. Similar result was reported in some recent studies and concluded the same [49, 50, 52].

TEM Analysis

The morphological and size dimensional characteristic of prepared silver nanoparticle was done using TEM analysis. Figure 3a represents the clustered/aggregated particle with each-other which was due to moisture gaining property of AgNPs, while Fig. 3b shows the typical image of spherical single AgNPs with an irregular surface. The size distribution of AgNPs was 50 to 130 nm found by TEM analysis which is also supported by SEM analysis. Kumar et al. [53] reported spherical shaped AgNPs with size dimension of

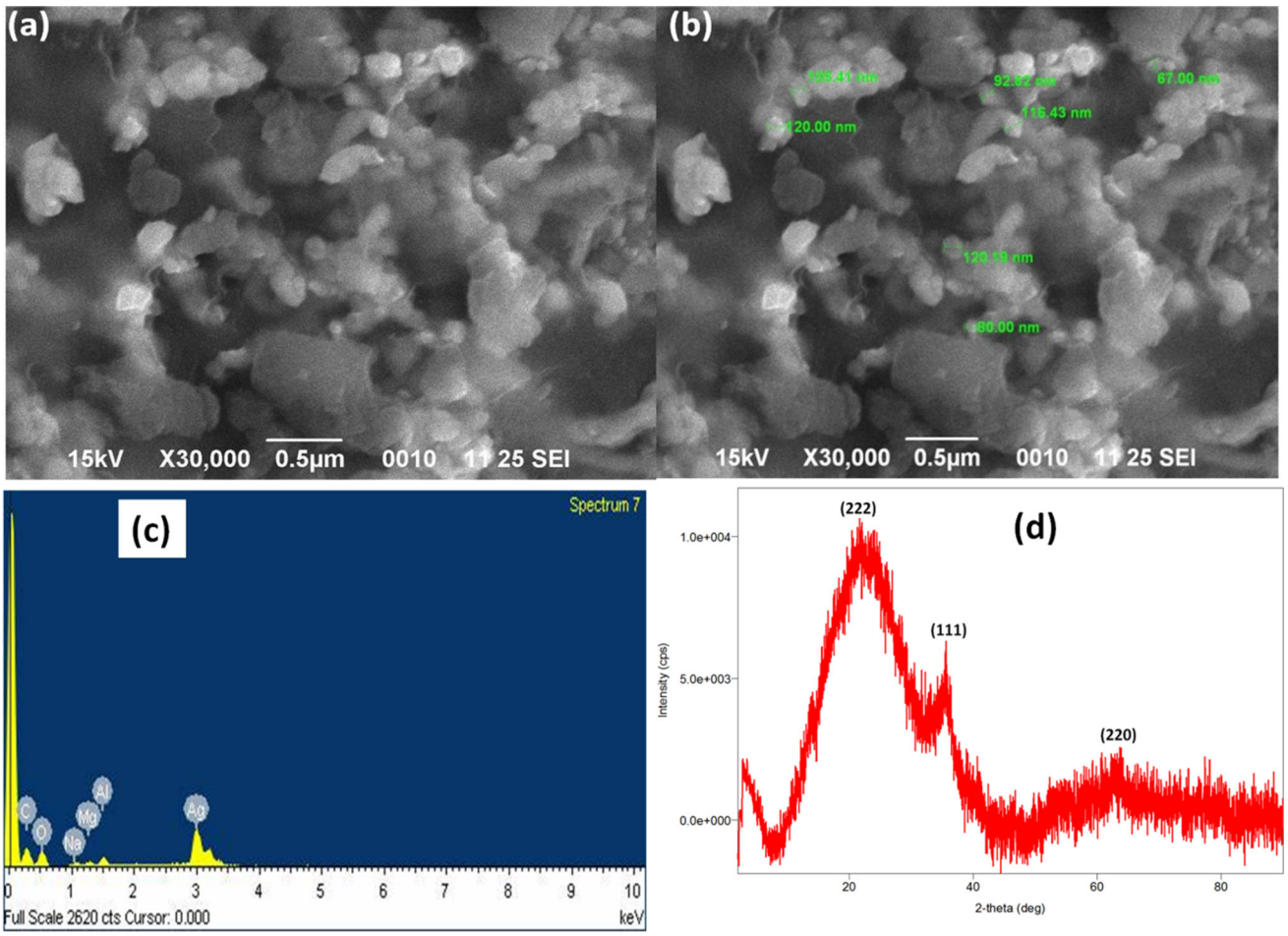

Fig. 1 **a** SEM analysis of synthesized AgNPs, **b** nano particle size distribution based on SEM analysis, **c** EDX Spectrum of silver nanoparticles and **d** XRD analysis of AgNPs

10–15 nm, prepared from Andean blackberry fruit extract. Dhand et al. [42] reported the spherical and ellipsoidal morphological AgNPs with size ranges from 20 to 150 nm, prepared using *Coffea arabica* seed extract. With spherical shape, smooth surface and average size (105.8 and 228.4 nm) AgNPs production was also reported using the extract of *Calligonum comosum* and *Fusarium* sp. [43].

Effect of AgNPs on Plant Pathogenic Fungi

Molecular Characterization of Pathogenic Fungal Isolate GPB

The ITS region sequence of *Rhizoctonia solani* isolate GPB was determined for phylogenetic analysis. *Rhizoctonia solani* isolate GPB showed closest relation with *Rhizoctonia solani* isolate AV4 and *R. solani* isolate RhCh-14 (Fig. 4). Neighbor-joining tree based on the ITS region sequence showed that isolate GPB made distinct branch with closely related species, *R. solani* isolate AV4 and *R. solani* RhCh-14 while the second branch carry *R. solani* IQ35, *Rhizoctonia* sp. AG-Fa, *R. solani* isolate aqeel3 and *R. solani* AG-Fa isolate SPM1 species of the genus *Rhizoctonia* (Fig. 4).

Antifungal Activity

The biologically synthesized silver nanoparticles showed excellent antifungal property against the fungus *Sclerotium rolfsii* and *Rhizoctonia solani* GPB. However, the antifungal activity of AgNPs varies with the nature of the fungus along with the properties of AgNPs such as size and shape [54]. Antifungal activity of AgNPs also has a close relation with the formation of pits in the cell wall of fungi [54]. According to Kim et al. [55], AgNPs affect fungal cell by attacking their membranes; thus, disrupting the membrane potential and causes cell death. Membrane damage due peroxidation was also reported in fungi via AgNPs activity [12] that might be a major cause of AgNPs lead to cell death.

In the present study, with increase in the concentration of AgNPs from 30 to 300 µg/L the inhibition percentage of

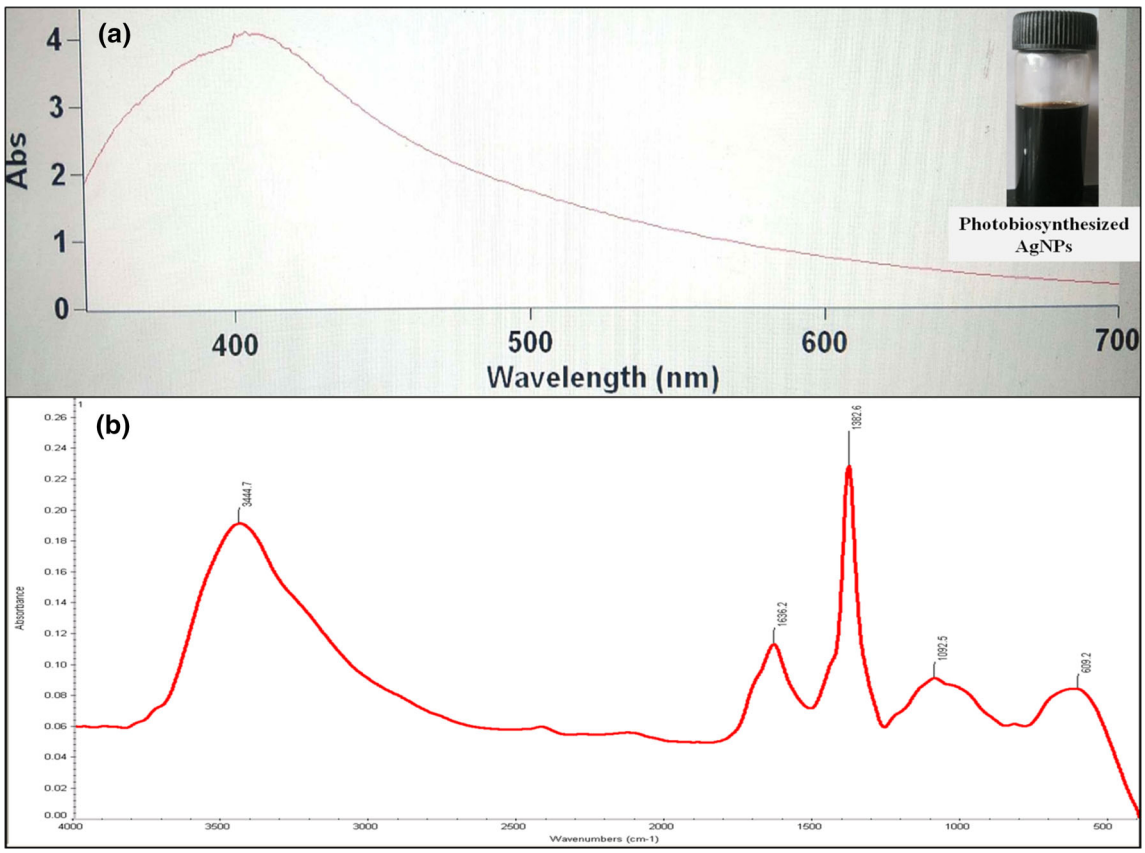

Fig. 2 **a** Detection of photobiosynthesized AgNPs using extract of *A. flavus* CR500 by UV–visible spectrophotometer and **b** FTIR spectra of AgNPs

Table 1 Detected FTIR bands and their assignments

S. no.	Peak (cm^{-1})	Assignment
1.	3444.7	–OH and –NH stretching
2.	1636.2	C=O stretching
3.	1382.6	COOH stretching
4.	1092.5	Phosphate stretching
5.	609.2	SO_2 stretching in sulphones

S. rolfsii was significantly ($p \leq 0.05$) increased from 56 to 100% at 6th day after incubation (Fig. 5). However, the growth of the *R. solani* was first instantly inhibited by 60% at 30 µg/L and above 30 µg/L of AgNPs, slow growth inhibition rate was recorded, which was 68, 75 and 83% at the concentration of 60, 90 and 120 µg/L of AgNPs respectively, at 6th day after incubation. A complete inhibition of the growth of *R. solani* GPB was found at 150 µg/L of AgNPs. For the complete growth inhibition of *Aspergillus nomius*, *A. flavus* and *A. parasiticus*, 78 µg/L of AgNPs were required [44]. Khatami et al. [56] synthesized the silver nanoparticle from waste-grass and 55 and 43% inhibition of the growth of *R. solani* and *Fusarium solani* was reported at the concentration of 20 µg/L. In this study, increase in the inhibition percentage with increase in the AgNPs concentration was due to ROS production (Table 2) [12]. It was also found that with increase in the incubation period from 2nd to 6th day, the inhibition percent of *S. rolfsii* at 150 µg/L of AgNPs was significantly ($p < 0.05$) decreased from 100 to 84% (Fig. 5), which might be due to increase in the antioxidative response with increase in the incubation period that relived the oxidative stress toxicity to the cell of the *S. rolfsii*. To confirm this hypothesis, the activity of catalase and peroxidase was analyzed which showed a significant increase in CAT and POD activity (Table 2). Several researchers have reported the significant effect of AgNPs on the growth of plant pathogenic fungi [55, 57, 58].

Lipid Peroxidation

It is previously reported that lipid peroxidation was increased in green algae, higher plants and zebrafish liver under the exposure of AgNPs [20, 22, 23]. In the present study, with increase in the AgNPs concentration from 0 to 50 µg/L, the melondialdehyde (MDA) accumulation in *R. solani* GPB and *S. rolfsii* was significantly increased from

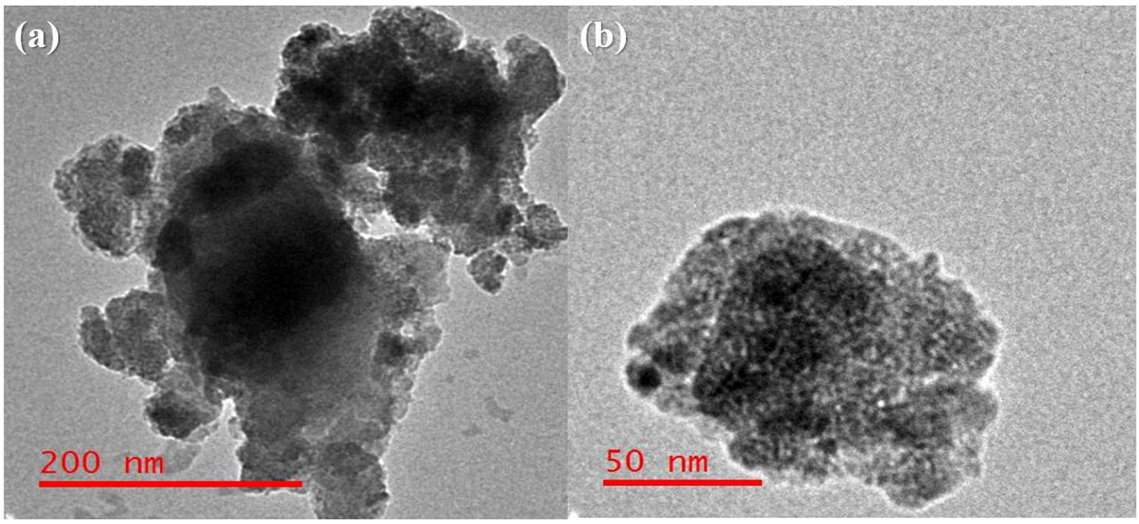

Fig. 3 TEM micrograph of photobiosynthesized silver nanoparticle using extract of *A. flavus* CR500 **a** aggregated or clustered and **b** single nanoparticle

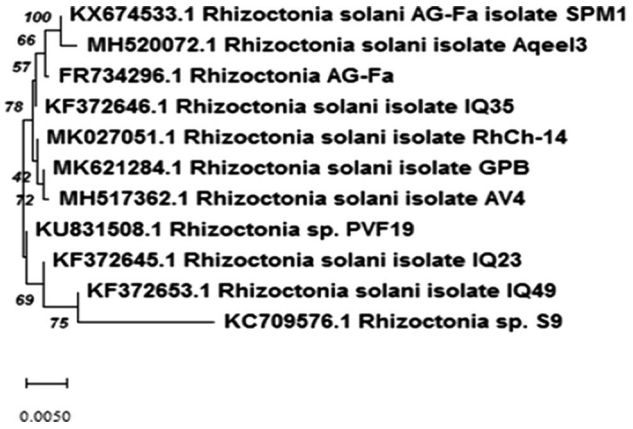

Fig. 4 Phylogenetic position of *Rhizoctonia solani* GPB along with other closely related species of the genus *Rhizoctonia*. The percentage of replicate trees in which the associated taxa clustered together in the bootstrap test (1000 replicates) are shown next to the branches. The tree was reconstructed using neighbor-joining analysis based on 654 bases of aligned ITS region sequences

1.53 ± 0.20 to 18.67 ± 1.01 and from 3.83 ± 0.35 to 32.2 ± 0.95 mU/mg of protein respectively (Table 2). However, MDA accumulation in *R. solani* GPB was higher than *S. rolfsii* at all the treatment which might be a primary cause of maximum inhibition at lower AgNPs concentration while severe inhibition of both fungi was recorded at higher concentration. Similar to our results, an increase in the MDA accumulation with increase in the AgNPs concentration was also reported in *Phanerochaete chrysosporium* [12]. The cause of inhibition due to reactive oxygen species production in presence of AgNPs was also reported in *Fusarium oxysporum*, *Alternaria brassicicola* and *Candida albicans* [11, 59]. The MDA is final product of lipid peroxidation due to reactive oxygen species production under environmental stress conditions (such as osmotic stress, heavy metal and drought) in plants and microbes [12, 19, 20, 31, 60]. Which can be taken into account to conclude it that severe inhibition in growth of *R. solani* GPB and *S. rofsii* is due to reactive oxygen species production in presence of AgNPs.

Antioxidant Response

The change in the activity of CAT in *R. solani* GPB and *S. rofsii* at different concentration of AgNPs is shown in

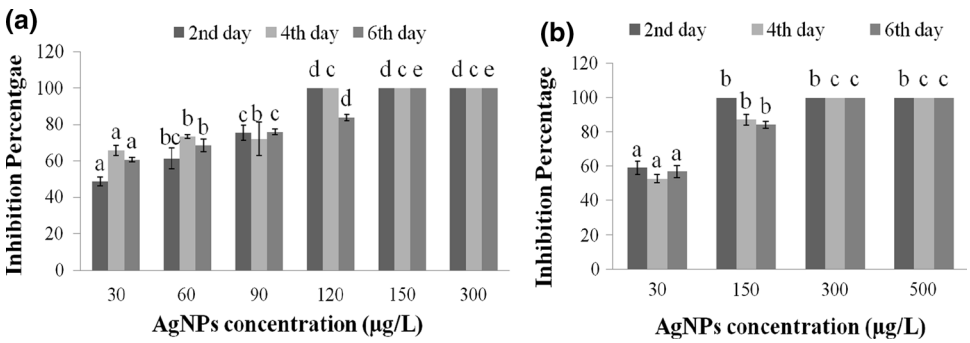

Fig. 5 Inhibition percentage of **a** *Rhizoctonia solani* GPB and **b** *Sclerotium rolfsii* at different concentration of photobiosynthesized AgNPs (mean ± standard deviation of three replicates followed by the same letter are not significantly different at the level of $p < 0.05_{DMRT}$)

Table 2 Effect of AgNPs on lipid peroxidation, activity of catalase and peroxidase in *S. rolfsii* and *R. solani* GPB (the values are presented as mean of three replicates ± standard deviation, same letter denote no significant difference at the level of $p < 0.05_{(DMRT)}$)

AgNPs concentration (µg/L)	Lipid Peroxidation (MDA) (mU/mg of prot)	Catalase (µM H_2O_2/min/mg prot)	Peroxidase (U/mg prot)
Sclerotium rolfsii			
0	3.83 ± 0.35^a	43 ± 2.64^a	2.26 ± 0.15^a
30	25.23 ± 0.90^b	114 ± 3.60^b	3.75 ± 0.32^b
50	32.2 ± 0.95^c	63.33 ± 3.51^c	4.10 ± 0.30^c
Rhizoctonia solani GPB			
0	1.53 ± 0.20^a	32.12 ± 2.0^a	1.33 ± 0.15^a
30	13.10 ± 0.52^b	96.33 ± 3.21^b	3.23 ± 0.15^b
50	18.67 ± 1.01^c	134.66 ± 3.51^c	5.26 ± 0.35^c

Table 2. The CAT activity was significantly increased when *R. solani* GPB and *S. rolfsii* came in the exposure of AgNPs. In *R. solani* GPB, CAT activity was increased significantly up to 114 ± 3.60 µM H_2O_2/min/mg protein at 30 µg/L and decrease with increase in the AgNPs concentration above 30 µg/L. However, in *S. rolfsii* the activity of CAT stimulated when come in the exposure of AgNPs and increased significantly from 32.12 ± 2.0 to 134.66 ± 3.51 µM H_2O_2/min/mg of protein with increase in the AgNPs concentration from 0 to 50 µg/L (Table 2). Huang et al. [12] investigated the effect of AgNPs on *Phanerochaete chrysosporium* and an increase in the activity of CAT in the presence of AgNPs was reported. The role of CAT was reported for scavenging of H_2O_2, produced under stress conditions [24, 45, 60–62] which clearly indicated the H_2O_2 and ROS production in the presence of AgNPs in both pathogenic fungi and also support the hypothesis that AgNPs produces reactive oxygen species in fungi and resulting oxidative stress leads to cell death. However, at lower concentration of AgNPs, *R. solani* GPB and *S. rofsii* showed strong antioxidant response but higher concentration of AgNPs may lead high amount of H_2O_2 and ROS induction that might higher than the antioxidative potential of fungi ultimately causes severe inhibition in growth of the fungi.

The change in the POD is implicated with the degradation of metabolizable constituents in microorganisms and their development [63]. In this study, the tendency in the activity of POD was similar to those of CAT activity in fungi with exposure of AgNPs. As well, the POD activity in *R. solani* was significantly increased to 5.26 U mg^{-1} protein followed by 4.10 U mg^{-1} protein in *S. rolfsii* at 50 µg/L of AgNPs (Table 2). The similar change in POD was also reported in *P. chrysosporium* in the exposure of AgNPs [12]. Antioxidants response as change in POD, SOD, CAT and GSH in the exposure of nanoparticle was also reported in plants and other microbes [2, 5, 12, 24, 64].

Effect of AgNPs on *V. radiata* and *C. arietinum* (Growth, Germination Rate, Lipid Peroxidation and Proline Content)

The nanoparticles application in crop disease management has many advantages but it may have negative impact on the crop development and production. With taking into account all the positive aspects of metallic nanoparticle in agricultural practices, the negative aspects such as stress and toxicity on the crop of these metallic nanoparticles should be thoroughly investigated. In this context the effect of AgNPs on germination rate and growth of *V. radiata* and *C. arietinum*, the lipid peroxidation and proline content was also measured, which has been previously reported in plant under the different stress condition such heavy metals [23, 24, 45, 60]. On another hand, to assess the AgNPs applicability for the seed protection via AgNPs coating, it is need to know interactive relation between seed and AgNPs whether it can affect the germination rate, growth and development of the crop or not.

The effect of AgNPs on the germination rate and growth of *V. radiata* and *C. arietinum* are shown in Fig. 6a, b. At all the tested AgNPs concentration, no significant change in germination rate and growth of *V. radiata* and *C. arietinum* was recorded compared to control treatment. The results suggest that the treatment of *V. radiata* and *C. arietinum* with AgNPs would not cause any inhibitory effect on the growth and development of the crops. For the assessment of the effect of the biogenic silver nanoparticle on the development of crop, Guilger et al. [34] used the Soybean seeds and reported the same results. Similar result on effect of AgNPs on germination rate was reported for Soybean by Spagnoletti et al. [5].

Further, to explore the AgNPs effect on the growth of seedling by means of biochemical impact, the proline and lipid peroxidation was assayed (Fig. 7). No significant change in proline and lipid peroxidation was observed in shoot of *V. radiata* and *C. arietinum* at all tested AgNPs

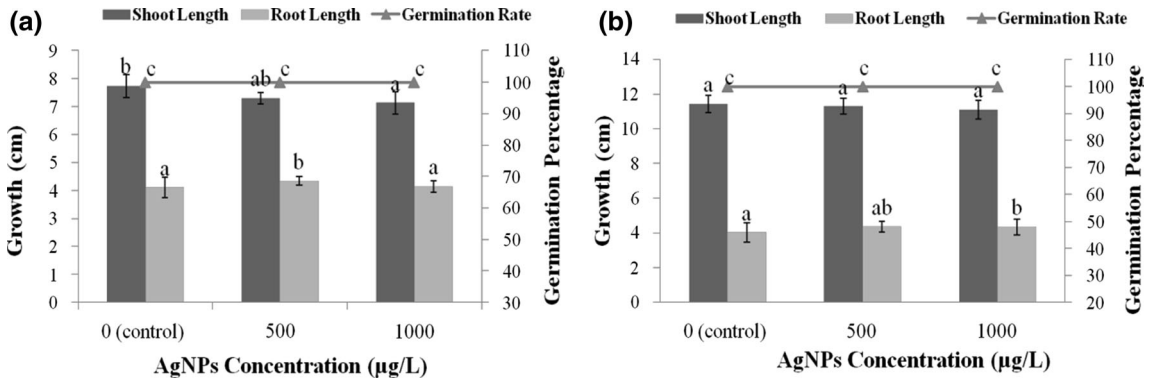

Fig. 6 Effect of photobiosynthesized AgNPs on the germination rate and growth of **a** *Cicer arietinum* and **b** *Vigna radiata* (mean ± standard deviation of three replicates followed by the same letter are not significantly different at the level of $p < 0.05_{DMRT}$)

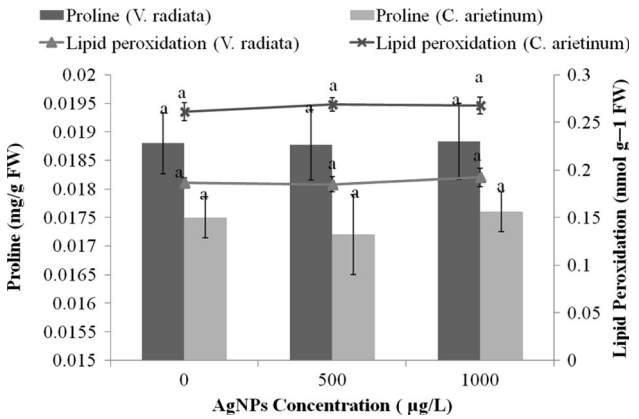

Fig. 7 Effect of synthesized AgNPs on Lipid peroxidation and proline content in seedling of *Vigna radiata* and *Cicer arietinum* (mean ± standard deviation of three replicates followed by the same letter are not significantly different at the level of $p < 0.05_{DMRT}$)

concentration compared to control treatment. Spagnoletti et al. [5] also reported the same results for lipid peroxidation under stress of AgNPs in soybean seeds. However, with increase in the AgNPs concentration up to 44 ppm, the decrease in lipid peroxidation was reported in seedlings of rice [2]. The decrease in lipid peroxidation was also reported in *Physalis peruviana* L. under AgNPs stress [64]. The results of this study revealed that photobiosynthesized AgNPs have not any negative impact on the growth and development of the *V. radiata* and *C. arietinum* and also AgNPs can be used for the seeds coating to protect the seeds from infectious diseases.

Conclusion

Photobiosynthesized AgNPs from extract of *Aspergillus flavus* CR500, with size 60–120 nm, crystalline nature and high functional group availability have very high potential to inhibit the growth of the plant pathogenic fungi *Rhizoctonia solani* GPB and *Sclerotium rolfsii* via producing reactive oxygen species. The assessment of the applicability of AgNPs for seed protection has not given any significant negative impact on the germination and growth of *Cicer arietinum* and *Vigna radiata* and also no considerable change was recorded in the lipid peroxidation and proline in their seedling growing in the exposure of AgNPs. Thus, photobiosynthesized AgNPs using the extract of *A. flavus* CR500 with efficient antifungal activity can be exploited on a large scale in an ecofriendly and economical way for crop disease management.

Acknowledgements The authors are thankful to the Head of the Department of Environmental Science, BBAU, Lucknow, India for providing Laboratory Facility. The authors are also thankful to National Centre for Microbial Resource (NCMR), Pune, India for providing Gene Sequencing Facility, the Director, USIC, BBAU, Lucknow for SEM and FTIR analysis and the support provided by Jiwaji University, Gwalior (M. P.) for XRD and TEM analysis. Two of us (Vinay Kumar and Ganesh Prasad) are grateful to UGC, New Delhi, India for providing fellowship.

Compliance with Ethical Standards

Conflict of interest The authors declare that they have no conflict of interest.

References

1. S. Mishra and H. B. Singh (2015). *Appl. Microbiol. Biotechnol.* **99**, 1097–1107.
2. S. D. Gupta, A. Agarwal, and S. Pradhan (2018). *Ecotoxicol. Environ. Saf.* **161**, 624–633.
3. F. Wang, Y. Hu, C. Guo, W. Huang, and C.-Z. Liu (2012). *Bioresour. Technol.* **110**, 120–124.
4. E. O. M. Ali, N. A. Shakil, V. S. Rana, D. J. Sarkar, S. Majumder, P. Kaushik, B. B. Singh, and J. Kumar (2017). *Ind. Crops Prod.* **108**, 379–387.
5. F. N. Spagnoletti, C. Spedalieri, F. Kronberg, and R. Giacometti (2019). *J. Environ. Manage.* **231**, 457–466.
6. A. Segorbe, E. D. Pietro, D. Pérez-Nadales, and D. Turrà (2017). *Mol. Plant Pathol.* **18**, 912–924.
7. F. E. Hartmann, A. Sánchez-Vallet, B. A. McDonald, and D. Croll (2017). *ISME J.* **11**, 1189–1204.

8. Y. Wang, P. Westerhoff, and K. D. Hristovski (2012). *J. Hazard. Mater.* **201**, 16–22.
9. A. U. Khan, N. M. M. Khan, M. H. Cho, and M. M. Khan (2018). *Bioprocess Biosyst. Eng.* **41**, 1–20.
10. S. Chowdhury, A. Basu, and S. Kundu (2014). *Nanoscale Res. Lett.* **9**, (1), 365.
11. S. Radhakrishnan, D. B. Munuswamy, Y. Devarajan, and A. Mahalingam (2018). *Energy Sour. A Recov. Util. Environ. Effects* **40**, (20), 2485–2493.
12. Z. Huang, K. He, Z. Song, G. Zeng, A. Chen, L. Yuan, H. Li, L. Hu, Z. Guo, and G. Chen (2018). *Chemosphere* **211**, 573–583.
13. N. Pantidos and L. E. Horsfall (2014). *J. Nanomed. Nanotechnol.* **5**, (5), 1.
14. A. T. Khalil, M. Ovais, I. Ullah, M. Ali, Z. K. Shinwari, D. Hassan, and M. Maaza (2018). *Artif. Cells Nanomed. Biotechnol.* **46**, (4), 838–852.
15. N. Jain, A. Bhargava, S. Majumdar, J. Tarafdar, and J. Panwar (2011). *Nanoscale* **3**, 635–641.
16. N. Durán, R. Cuevas, L. Cordi, O. Rubilar, and M. C. Diez (2014). *Springer Plus* **3**, (1), 645.
17. S. Prabhu and E. K. Poulose (2012). *Int. Nano Lett.* **2**, 1–10.
18. F. M. Christensen, H. J. Johnston, V. Stone, R. J. Aitken, S. Hankin, S. Peters, and K. Aschberger (2010). *Nanotoxicology* **4**, 284–295.
19. A. Chen, G. Zeng, G. Chen, L. Liu, C. Shang, X. Hu, L. Lu, M. Chen, Y. Zhou, and Q. Zhang (2014). *Process Biochem.* **49**, (4), 589–598.
20. J. E. Choi, S. Kim, J. H. Ahn, P. Youn, J. S. Kang, J. Yi, and D. Y. Ryu (2010). *Aquat. Toxicol.* **100**, (2), 151–159.
21. S. Arora, J. Jain, J. M. Rajwade, and K. M. Paknikar (2009). *Toxicol. Appl. Pharmacol.* **236**, 310–318.
22. A. Oukarroum, S. Bras, F. Perreault, and R. Popovic (2012). *Ecotoxicol. Environ. Saf.* **78**, 80–85.
23. H. S. Jiang, X. N. Qiu, G. B. Li, W. Li, and L. Y. Yin (2014). *Environ. Toxicol. Chem.* **33**, (6), 1398–1405.
24. V. Kumar and S. K. Dwivedi (2019). *Chemosphere*. https://doi.org/10.1016/j.chemosphere.2019.124567.
25. M. G. Babu and P. Gunasekaran (2009). *Colloids Surf. B* **74**, (1), 191–195.
26. G. Prasad and S. K. Dwivedi (2017). *EJBPS* **4**, (7), 478–481.
27. J. Sambrook, E. F. Fritsch, and T. Maniatis *Molecular Cloning a laboratory manual* (Cold Spring Harbor Laboratory Press, New York, 1989).
28. J. H. White, A. Wise, M. J. Main, A. Green, N. J. Frasae, G. H. Disney, A. A. Barnes, P. Emosan, S. M. Foord, and S. H. Marshall (1998). *Nature* **396**, 679–682.
29. G. M. Boratyn, C. Camacho, P. S. Cooper, G. Coulouris, A. Fong, N. Ma, T. L. Madden, W. T. Matten, S. D. McGinnis, Y. Merezhuk, Y. Raytselis, E. W. Sayers, T. Tao, J. Ye, and I. Zaretskaya (2013). *Nucleic Acids Res.* **41**, W29–W33.
30. S. Kumar, G. Stecher, M. Li, C. Knyaz, and K. Tamura (2018). *Mol. Biol. Evol.* **35**, 1547–1549.
31. F. Q. Zhang, Y. S. Wang, Z. P. Lou, and J. D. Dong (2007). *Chemosphere* **67**, (1), 44–50.
32. J. Xu (2010). *Plant Physiol.* **154**, 1319–1334.
33. Z. J. Zhu, G. Wei, J. Li, Q. O. Qian, and J. Q. Yu (2004). *Plant Sci.* **167**, 527–533.
34. M. Guilger, T. Pasquoto-Stigliani, N. Bilesky-Jose, R. Grillo, P. C. Abhilash, L. F. Fraceto, and R. de Lima (2017). *Sci. Rep.* **7**, 44421. https://doi.org/10.1038/srep44421.
35. A. Kannan and R. K. Upreti (2008). *J. Hazard. Mater.* **153**, 609–615.
36. P. L. Gratão, C. C. Monteiro, R. F. Carvalho, T. Tezotto, F. A. Piotto, L. E. Peres, and R. A. Azevedo (2012). *Plant Physiol. Biochem.* **56**, 79–96.
37. D. T. Plummer *Introduction to Practical Biochemistry* (Tata McGraw Hill Publishing 640 Co. Ltd, London, 1979).
38. D. K. Verma, S. H. Hasan, and R. M. Banik (2016). *J. Photochem. Photobiol. B* **155**, 51–59.
39. V. Kumar, D. K. Singh, S. Mohan, and S. H. Hasan (2016). *J. Photochem. Photobiol. B* **155**, 39–50.
40. J.-H. Lee, J.-M. Lim, P. Velmurugan, Y.-J. Park, Y.-J. Park, K.-S. Bang, and B.-T. Oh (2016). *J. Photochem. Photobiol. B* **162**, 93–99.
41. R. Al-Bahrani, J. Raman, H. Lakshmanan, A. A. Hassan, and V. Sabaratnam (2017). *Mater. Lett.* **186**, 21–25.
42. V. Dhand, L. Soumya, S. Bharadwaj, S. Chakra, D. Bhatt, and B. Sreedhar (2016). *Mater. Sci. Eng. C* **58**, 36–43.
43. A. E. Mohammed, F. F. B. Baz, and J. S. Albrahim (2018). *3 Biotech* **8**, 72.
44. K. P. Bocate, G. F. Reis, P. C. de Souza, A. G. O. Junior, N. Durán, G. Nakazato, and L. A. Panagio (2019). *Int. J. Food Microbiol.* **291**, 79–86.
45. V. Kumar, S. Singh, G. Singh, and S. K. Dwivedi (2019). *Geomicrobiol. J.* **36**, (9), 782–791.
46. S. Neethu, S. J. Midhun, M. A. Sunil, S. Soumya, E. K. Radhakrishnan, and M. Jyothis (2018). *J. Photochem. Photobiol. B* **180**, 175–185.
47. A. Saravanakumar, M. M. Peng, M. Ganesh, J. Jayaprakash, M. Mohankumar, and H. T. Jang (2017). *Artif. Cells Nanomed. Biotechnol.* **45**, (6), 1165–1171.
48. S. Basavaraja, S. D. Balaji, A. Lagashetty, A. H. Rajasab, and A. Venkataraman (2008). *Mater. Res. Bull.* **43**, (5), 1164–1170.
49. M. Wojnicki, T. Tokarski, V. Hessel, K. Fitzner, and M. Luty-Błocho (2019). *J. Flow Chem.* **9**, (1), 1–7.
50. H. Yang, Y. Wang, X. Chen, X. Zhao, L. Gu, H. Huang, J. Yan, C. Xu, G. Li, J. Wu, A. J. Edwards, B. Dittrich, Z. Tang, D. Wang, L. Lehtovaara, H. Häkkinen, and N. Zheng (2016). *Nat. Commun.* **7**, 12809.
51. K. Rajaram, D. C. Aiswarya, and P. Sureshkumar (2015). *Mater. Lett.* **138**, 251–254.
52. K. Anandalakshmi, J. Venugobal, and V. Ramasamy (2016). *Appl. Nanosci.* **6**, (3), 399–408.
53. B. Kumar, S. Kumari, L. Cumbal, and A. Debut (2015). *Asian Pac. J. Trop. Biomed* **5**, (3), 192–195.
54. A. Shafaghat (2015). *Synth. React. Inorg. M.* **45**, (3), 381–387.
55. J. S. Kim, E. Kuk, K. N. Yu, J. H. Kim, S. J. Park, H. J. Lee, S. H. Kim, Y. K. Park, Y. H. Park, C. Y. Hwang, and Y. K. Kim (2007). *Nanomed. Nanotechnol. Biol. Med.* **3**, (1), 95–101.
56. M. Khatami, I. Sharifi, M. A. Nobre, N. Zafarnia, and M. R. Aflatoonian (2018). *Green Chem. Lett. Rev.* **11**, (2), 125–134.
57. H. J. Park, S. H. Kim, H. J. Kim, and S. H. Choi (2006). *Plant Pathol. J.* **22**, (3), 295–302.
58. J. S. Min, K. S. Kim, S. W. Kim, J. H. Jung, K. Lamsal, S. B. Kim, M. Y. Jung, and Y. S. Lee (2009). *Plant Pathol. J.* **25**, (4), 376–380.
59. M. Kumari, V. P. Giri, S. Pandey, M. Kumar, R. Katiyar, C. S. Nautiyal, and A. Mishra (2019). *Pestic. Biochem. Phys.* **157**, 45–52.
60. J. Xu, Y. Y. Zhu, Q. Ge, Y. L. Li, J. H. Sun, Y. Zhang, and X. J. Liu (2012). *New Phytol.* **196**, (1), 125–138.
61. G. Prasad, V. Kumar, and S. K. Dwivedi (2018). *Asian J. Biol. Sci.* **13**, 21–27.
62. V. Kumar and S. K. Dwivedi (2019). *Ecotoxicol. Environ. Saf.*. https://doi.org/10.1016/j.ecoenv.2019.109734.
63. C. Serra-Wittling, S. Houot, and E. Barriuso (1995). *Biol. Fertil. Soils* **20**, (4), 226–236.
64. C. D. O. Timoteo, R. Paiva, M. V. Reis, P. I. C. Claro, L. M. Ferraz, J. M. Marconcini, and J. E. de Oliveira (2019). *3 Biotech* **9**, 145.